Journal of Materials Chemistry C

COMMUNICATION

View Article Online
View Journal

Improvement of bias stability of oxyanion-incorporated aqueous sol–gel processed indium zinc oxide TFTs†

Cite this: DOI: 10.1039/c4tc00667d

Received 2nd April 2014
Accepted 4th June 2014

DOI: 10.1039/c4tc00667d

www.rsc.org/MaterialsC

Hyungjin Park,‡ YunYong Nam,‡ Jungho Jin and Byeong-Soo Bae*

Oxyanion-incorporated indium zinc oxide (IZO) TFTs exhibiting excellent bias stabilities are fabricated from aqueous IZO precursor solutions blended with a catalytic amount of inorganic acids (H_2SO_4, H_3PO_4, H_3BO_3). The resulting oxyanion-incorporated IZO TFTs (SO–IZO, PO–IZO, BO–IZO) exhibit improved bias stabilities under NBS, PBS, NBTS, and PBTS conditions.

Introduction

Amorphous metal oxide semiconductors have been extensively studied as the active layer of thin film transistors (TFTs) in the last decade, in order to complement amorphous silicon (a-Si), which has been the industrial standard. The metal oxide TFT is considered a promising candidate for the active matrix of liquid crystal displays (AMLCDs) and organic light emitting diode displays (AMOLEDs) due to their characteristics, such as high field-effect mobility, low sub-threshold swing, high current on/off ratio and transparency.

Recently, studies on the stability of oxide TFTs under actual operating conditions have drawn much attention. During operation of the driving circuits of AMLCD and AMOLED, either negative or positive bias is consistently applied to the gate electrode, which results in gradual shifts of the TFT turn-on voltage to the negative or positive, respectively. In addition to this gate bias stress, thermal stress is generated during operation, as well as illumination stress, caused by both internal (back light unit) and external light sources. These can cause a disruptive turn-on voltage shift and/or sub-threshold swing degradation. These stress-induced instabilities in oxide TFTs are major factors that cause imaging problems such as image burn-in or image retention.

Laboratory of Optical Materials and Coating (LOMC), Department of Materials Science and Engineering, Korea Advanced Institute of Science and Technology (KAIST), Daejeon 305-701, Korea. E-mail: bsbae@kaist.ac.kr

† Electronic supplementary information (ESI) available. See DOI: 10.1039/c4tc00667d

‡ Both authors contributed equally to this work.

In general, the stress-induced instabilities in oxide TFTs are intimately related to charge defects that inherently exist in the metal oxide channel layer. These charge defects include metal cationic interstitials, oxygen vacancies, and impurities. Among these charge defects, the oxygen vacancy is universally ascribed to be the origin of the instability, inasmuch as they generate distributed sub-gap traps, despite being sources for electron carriers. In this regard, most of the research studies on oxide TFT stability have focused on controlling the level of oxygen vacancies in the metal oxide channel layer.

As a rational approach, some have attempted to supply additional oxygen into the as-fabricated metal oxide layer – mostly vacuum-deposited thin films. In this approach, the as-fabricated metal oxide layer is subjected to a post-annealing process for additional oxygen supply such as annealing with higher oxygen partial pressure,[1] oxygen plasma,[2] and ozone.[3] These methods have reduced levels of oxygen deficiency and improved bias stability, although they require vacuum facilities for the two-step process. As another strategy, attempts to incorporate metal cations with higher binding energy for oxygen have been reported, and these approaches can be applied to both vacuum-deposited thin films as well as typical sol–gel derived thin films. For example, Hwang *et al.* reported that an aqueous sol–gel processed indium oxide TFT, when combined with Al, Ga and Zn, exhibits reliable bias stabilities.[4] However, incorporating such hetero metal cations also led to the creation of metal hydroxide impurities, resulting in limited improvements of TFT stability. The metal oxide layers included oxygen vacancies as well as metal hydroxide related species, and the resulting combination influenced the stability mechanism in different ways. The positive bias stability became worse, even though the negative bias became better due to the decrease in the amount of oxygen vacancies. Banger *et al.* investigated the effect of alkaline earth atoms such as Ba and Sr in indium zinc oxide (IZO) TFTs.[5] They synthesized alkyl metal alkoxide precursor solution under anaerobic conditions designated to the 'ink-on-demand process' and utilized dipping as-spun films into water for hydrolysis. Due to the high Gibbs energy of

oxidation and large cation radii, the quaternary IBZO and ISZO thin films with the controlled amount of deep oxygen trap states and the desirable amorphous phase were fabricated and resulting TFTs showed excellent electrical mobility with stable device performance under a constant current or voltage bias. Seo *et al.* incorporated fluorine into IZO (IZO:F) TFTs.[6] Fluorine as an anion played a unique role of negating charge defects – oxygen vacancies and hydroxyl related species – leading to improvement of the stability of IZO TFTs.

Herein, we report a one-pot solution process that enables the effective improvement of TFT stability of a typical sol–gel metal oxide semiconductor, indium zinc oxide (IZO). Network-forming oxyanions – sulfate (SO_4^{2-}), phosphate (PO_4^{3-}), and borate (BO_3^{3-}) – were introduced into the IZO framework as additional oxygen sources. The incorporation of oxyanions was readily achieved by the addition of sulfuric, phosphoric and boric acids into the indium zinc oxide precursor solution. Subsequent simple annealing of spin-coated films from each solution mixture produced dense metal oxide active channel layers with low oxygen vacancy levels and TFT characteristics exhibiting excellent performance stabilities. In this report, we discuss the synthesis and fabrication of oxyanion incorporated indium zinc oxide TFTs and characterize their electrical performance and stabilities.

Experimental

A 0.2 M aqueous indium zinc oxide (IZO) precursor solution was prepared by dissolving indium nitrate hydrate ($In(NO_3)_3 \cdot xH_2O$, Aldrich) and zinc nitrate hydrate ($Zn(NO_3)_2 \cdot xH_2O$, Aldrich) in 10 mL of deionized water. In order to optimize the electrical performance, the ratio of indium to zinc was fixed to 6 : 4 and sulfuric acid (H_2SO_4, 95%, Aldrich), phosphoric acid (H_3PO_4, 85%, Aldrich) or boric acid (H_3BO_3, 99.5%, Aldrich) was added into the IZO solution. Those precursor solutions were vigorously stirred at room temperature for 6 hours to make them transparent and homogeneous. For fabrication of the oxyanion incorporated IZO TFTs, SiO_2/p^+-Si substrates were used as gate dielectrics/gate after O_2 plasma (300 W) cleaning for 5 min. The precursor solutions were filtered through a 0.22 μm syringe filter [poly(tetrafluoroethylene), GE] and spin-coated at 5000 rpm for 30 s on the substrate. Then, the as-deposited films were annealed on a hotplate at 350 °C for 2 hours in an ambient atmosphere (17 °C, 35% of relative humidity). XRD analyses of the IZO and inorganic acid incorporated IZO thin films confirmed no crystalline phases (Fig. S1†). Source and drain electrodes (Al, 100 nm) were then deposited by an E-beam evaporator with a shadow mask. The channel width and length of the fabricated TFT devices were 1000 and 100 μm, respectively.

Chemical composition of the oxide films was examined by X-ray photoelectron spectroscopy (XPS, Sigma Probe, Thermo VG Scientific). The data were collected using monochromatic Al K radiation (1486.6 eV) in an ultra-high vacuum system with a base pressure of $\sim 10^{-10}$ Torr. The interiors of the films were analyzed after Ar sputtering for 15 s. The Ar 2p peak at 241.9 eV was used for the calibration. Transfer curves of the fabricated devices were measured at 40 V of gate bias in an ambient atmosphere using an HP 4156A precision semiconductor parameter analyzer. Bias stability (NBS and PBS) and bias-temperature stability (NBTS and PBTS) were recorded under a constant positive (+20 V) and negative (−20 V) gate bias with V_{DS} = 0 V for 0–3600 s at room temperature and under 60 °C conditions. For the stability measurement, V_{DS} was set to 20 V and V_G was swept from −20 V to 20 V.

Results

Fig. 1 displays transfer curves of SO–I_6Z_4O, PO–I_6Z_4O, and BO–I_6Z_4O TFTs, and Table 1 summarizes the optimal compositions for each TFTs with their electrical performance. The I_6Z_4O TFT shows a high off-current ($\sim 10^{-8}$ A) and a turn-on voltage (V_{ON}) of −6 V, showing typical TFT characteristics for an indium-rich device.[6,7] Incorporation of a catalytic amount of oxyanion results in a decrease in mobility and higher current on/off ratio with clearly better swing performances, which is ascribed to reduction in electron carriers and the sub-gap states in the vicinity of the Fermi-level. However, further increase of oxyanion contents may cause disruption of the original IZO network and the oxyanion could act as impurities, resulting in a decrease of the overall current level coupled with positive V_{ON} shifts (Fig. S3†).

Bias stabilities of SO–I_6Z_4O, PO–I_6Z_4O, and BO–I_6Z_4O TFTs were investigated under NBS, PBS, NBTS, and PBTS conditions (Fig. 2 and Table 2). Here, we chose an I_5Z_5O TFT as the control device for the stability tests since the TFT stability of the I_6Z_4O composition is too much sensitive under bias stress conditions. The I_5Z_5O TFT showed a shift of −2.2 V upon the NBS and +3.4 V upon the PBS after 3600 s. Generally, an n-type oxide TFT, whose major carriers are electrons with higher carrier trapping probability than hole carriers, shows worse stability under PBS conditions than under NBS conditions.[8] As summarized in Table 2, when a negative gate bias was applied to the SO-, PO- and BO-I_6Z_4O TFTs, V_{ON} was shifted by −0.63 V, −0.8 V and −1.18 V, respectively, and for the positive gate bias, V_{ON} was shifted by +0.67 V, +1.2 V and +2.8 V, respectively.

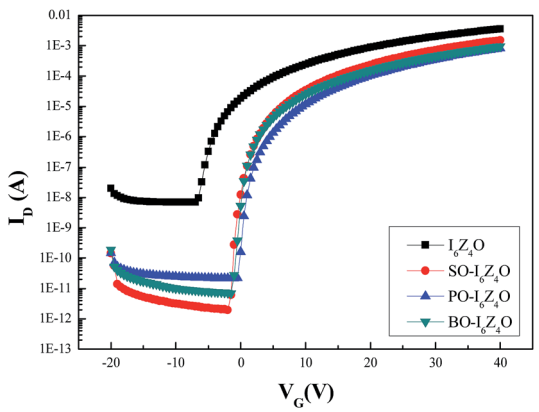

Fig. 1 Transfer characteristics of oxyanion-incorporated I_6Z_4O TFTs. All the curves are recorded under negative to positive voltage sweep conditions (V_{DS} = 40 V). See Fig. S2† for corresponding output curves.

Table 1 Optimal compositions for oxyanion incorporated IZO thin films and their TFT characteristics

	Composition					TFT characteristics			
	$In(NO_3)_3 \cdot xH_2O$	$Zn(NO_3)_2 \cdot xH_2O$	H_2SO_4	H_3PO_4	H_3BO_3	Mobility	V_{ON}	I_{on}/I_{off}	S.S.
I_5Z_5O[a]	0.10 M	0.10 M	—	—	—	13.0 $cm^2 V^{-1} s^{-1}$	0 V	$\sim 10^8$	0.41 V per decade
I_6Z_4O[b]	0.12 M	0.08 M	—	—	—	20.3 $cm^2 V^{-1} s^{-1}$	−6 V	$\sim 10^5$	0.78 V per decade
SO–I_6Z_4O	0.12 M	0.08 M	0.01 M	—	—	8.1 $cm^2 V^{-1} s^{-1}$	−1 V	$\sim 10^8$	0.30 V per decade
PO–I_6Z_4O	0.12 M	0.08 M	—	0.01 M	—	6.3 $cm^2 V^{-1} s^{-1}$	0 V	$\sim 10^7$	0.42 V per decade
BO–I_6Z_4O	0.12 M	0.08 M	—	—	0.02 M	7.9 $cm^2 V^{-1} s^{-1}$	−1 V	$\sim 10^8$	0.44 V per decade

[a] Reference for the stability test. [b] Reference for optimal electrical performance.

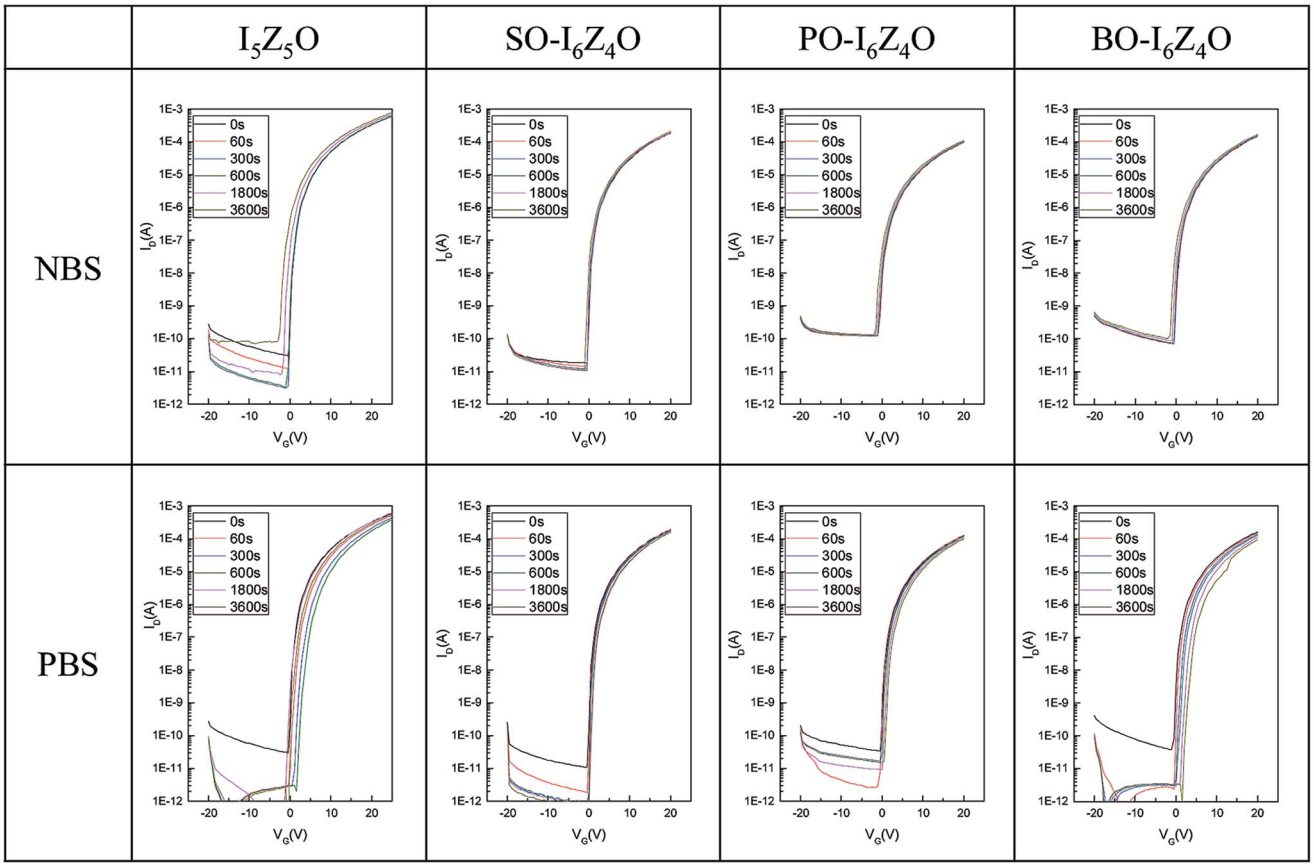

Fig. 2 NBS and PBS stability tests of I_5Z_5O and oxyanion-incorporated I_6Z_4O TFTs.

Table 2 Values of ΔV_{ON} ($V_{ON,Final} - V_{ON,Initial}$) of I_5Z_5O TFTs and optimized inorganic acid incorporated I_6Z_4O TFTs under NBS, NBTS, PBS and PBTS conditions after 3600 s

Composition	NBS	NBTS	PBS	PBTS
I_6Z_4O	−3.5 V	—	+4.9 V	—
I_5Z_5O	−2.2 V	−12.2 V	+3.4 V	>+20 V
SO–I_6Z_4O	−0.6 V	−3.3 V	+0.7 V	+1.5 V
PO–I_6Z_4O	−0.8 V	−3.4 V	+1.2 V	+1.8 V
BO–I_6Z_4O	−1.2 V	−6.3 V	+2.8 V	+3.0 V

Bias stabilities of the oxyanion-incorporated IZO TFTs under an additional thermal stress (BTS, $T = 60$ °C) were also examined (Table 2). The oxyanion-incorporated IZO TFTs showed more stable TFT performances ($\Delta V_{ON} = -3.35$ V, −3.4 V and −6.34 V, respectively) than I_5Z_5O ($\Delta V_{ON} = -12.2$ V) under NBTS conditions. Similarly, stabilities of the oxyanion-incorporated IZO TFTs under PBTS conditions were superior to the I_5Z_5O TFT of which ΔV_{ON} was even greater than +20 V.

Discussion

The precursor solution for the base IZO matrix was prepared by dissolving indium nitrate and zinc nitrate in deionized water. It has been reported that when metal nitrate is dissolved in water, the metal cation becomes solvated by water molecules, forming a metal aquo complex (Fig. 3a). For indium nitrate, an indium cation forms an indium complex with hexa-aquo ligands

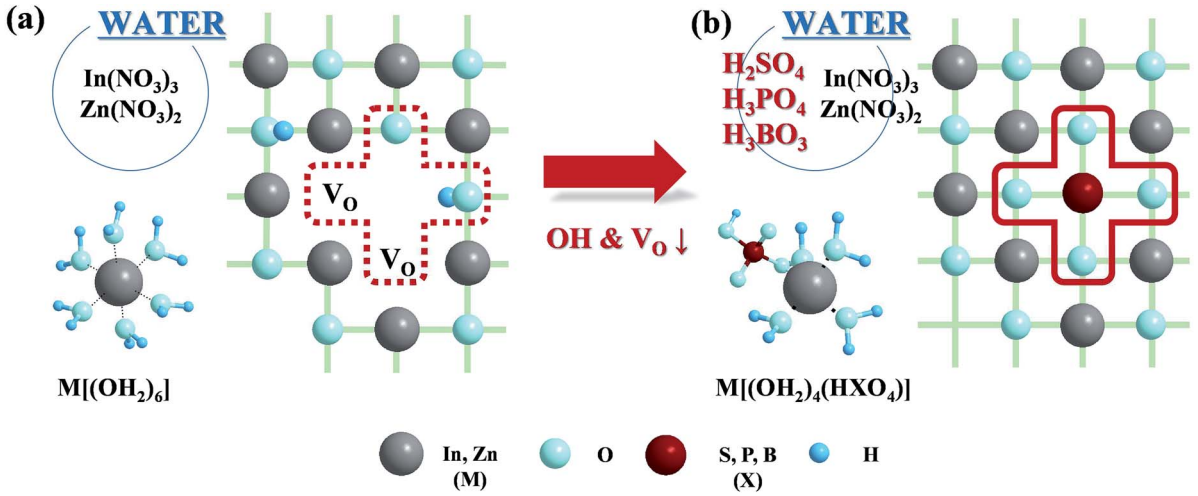

Fig. 3 Scheme for controlling hydroxyl groups and oxygen vacancies by incorporating inorganic acids (sulfuric acid, phosphoric acid and boric acid) into the IZO film. (a) The metal–aquo ligand is the building block of a metal oxide thin film. Oxygen vacancies and hydroxyl residues are inevitable because they originate from the aqueous route indium oxide based film. (b) As a result of acid incorporation, oxyanions are strongly attached to the metal atoms, replacing several aquo ligands. They can survive thermal annealing and work as network formers, providing additional oxygen atoms to the IZO film.

$[In(H_2O)_6^{3+}]$.[9] These aquo ligands undergo thermohydrolysis in the subsequent annealing process for thin film fabrication, during which the aquo groups transform to hydroxyl and/or oxo ligands and the final thin film ends up with M–OH–M or M–O–M frameworks as a result of sol–gel condensation.[10] As discussed earlier, either these residual hydroxyls (–OH) or the excess of oxygen vacancies (V_O) due to incomplete condensation become major sources for bias-induced TFT instabilities. As such, in typical metal oxide TFTs, it is important to effectively reduce hydroxyl residues and promote the formation of metal–oxygen bonds in order to improve bias-induced stabilities.

As a one-pot solution approach that enables improved bias stabilities of the IZO TFT, we incorporated oxyanions of sulfate (SO_4^{2-}), phosphate (PO_4^{3-}), and borate (BO_3^{3-}) into the base IZO network by adding sulfuric, phosphoric and boric acid to the aqueous IZO solution (Fig. 3b). The introduction of such oxyanions into the main IZO framework is expected to be beneficial for the following two reasons.

(i) Oxyanions are capable of reducing V_O & –OH

The incorporated inorganic acids are capable of forming bi- or tri-valent oxyanions, such as sulfate (SO_4^{2-}), phosphate (PO_4^{3-}) and borate (BO_3^{3-}). These oxyanions have high complexing ability with adjoining indium or zinc cations by replacing some of their aquo ligands,[11–13] thereby limiting the chance of creating –OH impurities. HR-MS analyses of the acid incorporated indium nitrate solution reveal some heavier molecular species than the aquo indium complex derivatives, suggesting

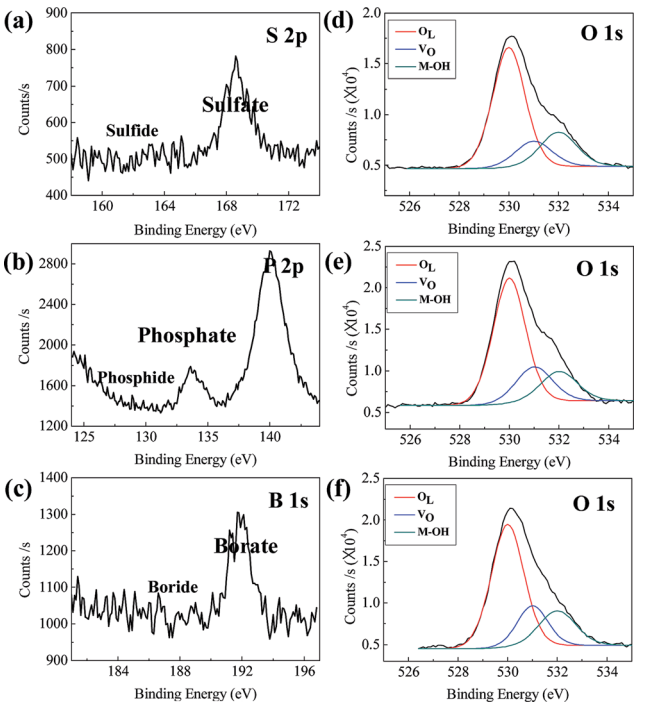

Fig. 4 XPS spectra of (a and d) SO–I_6Z_4O, (b and e) PO–I_6Z_4O, and (c and f) BO–I_6Z_4O thin films. In (b), the Zn 3s peak at 140 eV intervened in P 2p spectra.

Table 3 Quantitative analysis of XPS O 1s spectra of the I_6Z_4O and oxyanion incorporated I_6Z_4O films

	530 eV (M–O–M or X[a])	531.5 eV (V_O)	532 eV (M–OH & oxyanion)
I_6Z_4O	45.1%	30.7%	24.2%
SO–I_6Z_4O	64.6%	14.8%	20.5%
PO–I_6Z_4O	63.3%	19.0%	17.6%
BO–I_6Z_4O	61.3%	19.2%	19.5%

[a] X = S,P, or B.

the existence of indium complexes with oxyanion ligands (Fig. 3b and S4†). These oxyanions (SO_4^{2-}, PO_4^{3-}, BO_3^{3-}) carry additional oxygen atoms and can provide more oxygen in the final oxide thin film, reducing oxygen vacancy (V_O).

(ii) Oxyanions are network formers

The oxyanions themselves can also function as network formers which can bridge more than two cations without the expense of a condensation reaction.[13] Fig. 3b illustrates a schematic oxide network structure, where an oxyanion links adjacent metal cations by forming M–O–X–O–M bonds (X = S, P, B) in the IZO film after thermal annealing. Since the bonding energies of S, P and B with oxygen are higher – 521.7 kJ mol^{-1}, 599.1 kJ mol^{-1} and 808.8 kJ mol^{-1}, respectively – than those of In–O and Zn–O (320.1 kJ mol^{-1} and 159 kJ mol^{-1}, respectively),[14] it is highly likely that the network-forming oxyanions remain stable in the IZO network. All the oxyanion-incorporated IZO thin-films are confirmed to be free of nitrogen contamination (Fig. S5†).

The existence of oxyanion in the IZO network was confirmed by XPS (Fig. 4). In Fig. 4a, the characteristic peak at 162 eV for S^{2-} species in the form of a metal–sulfur bond (sulfide) is absent and instead a clear peak assigned to positively charged S^{6+} (*i.e.*, sulfate ion with four surrounding oxygen atoms) is observed.[15,16] Similarly, in the P 2p and B 1s spectra (Fig. 4b and c), the characteristic peaks corresponding to phosphate (~133 eV) and borate (~192 eV) anions are shown instead of phosphide and boride, respectivley.[17,18] These results verify the existence of oxyanions in the final IZO thin film.

Fig. 4d–f are O 1s peaks of SO-, PO- and BO-I_6Z_4O films. The O 1s peaks are deconvoluted to 530 eV, 531.5 eV and 532 eV denoting oxygen in oxide lattices (M–O–M), oxygen vacancy in lattices (V_O) and oxygen in hydroxide-related species (M–OH), respectively.[8,9] As expected from Fig. 3, quantitative analyses from the XPS results (Table 3) reveal an increased fraction of lattice oxygen atoms and a decrease of oxygen vacancy (V_O), which is due to the additional supply of oxygen atoms from the incorporated oxyanions. Moreover, the oxyanion-incorporated IZO TFTs are characterized with a reduced level of hydroxide species. However, the degree of the reduction is less evident due to the overlapping of the characteristic binding energy for hydroxide species and oxyanions (532 eV).[19–22]

The instability of electrical properties under gate bias stress can be explain by two general mechanisms: (1) the defect creation model[23,24] and (2) the charge trapping model.[25] In the defect creation model, degradation of sub-threshold swing occurs as a result of gate bias stress that causes creation of trap sites. In the charge trapping model, on the other hand, charge carriers are trapped at the dielectric/channel interface and inside the channel. These trapped carriers screen applied gate bias, typically resulting in parallel shift of the transfer curve without significant change in the sub-threshold swing. The charge trapping model relates the turn-on voltage shift ($\Delta V_{ON} = V_{ON,Final} - V_{ON,Initial}$) and stress time by the following stretched-exponential equation;[4,26]

$$\Delta V_{ON} = \Delta V_{ON0}[1 - \exp\{-(t/\tau)^{\beta}\}]$$

where ΔV_{ON0} is the ΔV_{ON} at infinite time, τ is the characteristic trapping time of electron carriers, and t is the stress duration time. As shown in Fig. 2, the transfer curves of optimized SO-, PO-, and BO-I_6Z_4O TFTs show no degradation of sub-threshold swing with only little parallel shift. This suggests that bias stabilities of oxyanion-incorporated IZO TFTs are governed by the charge trapping model. Fitting ΔV_{ON} with the above equation further confirms that the bias-instabilities of oxyanion-incorporated IZO TFTs result from the charge trapping mechanism (Fig. S6†).

In oxyanion-incorporated IZO TFTs, the reduction in both V_O and M–OH represents the overall decrease in the charge trapping center,[27] which allows effective attenuation of the screening effect of applied gate bias upon actual TFT operation. From Fig. 2 and Table 2, it is noteworthy that SO-, PO- and BO-I_6Z_4O TFTs show prominent improvements under both NBS and PBS conditions. Under PBS conditions, oxygen-related defects such as M–OH and unoccupied V_O ($V_O^{\cdot\cdot}$) created by donating an electron generate shallow trap states below the conduction band minimum (CBM). Under PBS condition, these defects can capture electron carriers from the conduction band. This causes the screening of applied gate bias and as a result a larger positive bias is required for turning-on TFTs.[28] On the other hand, occupied V_O generates deep trap states that are widely distributed above the valence band maximum (VBM). Under NBS condition, a negative bias stress induces hole trapping at the deep level traps and a larger negative bias is required.[29,30] Consequently, the improvements of bias stability of oxyanion-incorporated IZO TFTs under both NBS and PBS conditions are attributed to the reduced level of oxygen-related defects (*i.e.*, charge traps) that have negative impact on bias stability.

From Table 2, incorporation of sulfate oxyanion (SO_4^{2-}) is likely to be the most effective for improving bias stability of IZO TFTs. This is thought to be due to higher electronegativity of sulfate ($\chi = 3.27$) than those of phosphate and borate ($\chi = 3.19$ and 3.09, respectively).[31] The larger difference between electronegativity of a sulfate oxyanion and the metal atom (1.78 for In and 1.65 for Zn) leads to a stronger metal–oxyanion bond.

Conclusions

In summary, we have fabricated a series of oxyanion-incorporated IZO TFTs exhibiting excellent bias stabilities from aqueous IZO precursor solutions blended with a catalytic amount of inorganic acids (H_2SO_4, H_3PO_4, and H_3BO_3). In the aqueous sol–gel derived thin-film formation at 350 °C, the inorganic acids are incorporated into the IZO network as oxyanions (SO_4^{2-}, PO_4^{3-}, and BO_3^{3-}). These network-forming oxyanions effectively reduce the inherent oxygen-related defects (oxygen vacancy and hydroxyls) which are the main cause for bias instability of typical oxide TFTs, resulting in improved bias stability under NBS, PBS, NBTS, and PBTS conditions.

Acknowledgements

This work was supported by the Materials Original Technology Program (10041222) funded by the Ministry of Knowledge

Economy (MKE, Korea) and the National Research Foundation of Korea (NRF) grant funded by the Korea government (MSIP) (CAFDC 5-3, NRF-2007-0056090).

Notes and references

1 K. H. Ji, J.-I. Kim, H. Y. Jung, S. Y. Park, R. Choi, U. K. Kim, C. S. Hwang, D. Lee, H. Hwang and J. K. Jeong, *Appl. Phys. Lett.*, 2011, **98**, 103509.
2 S. Yang, K. H. Ji, U. K. Kim, C. S. Hwang, S.-H. Ko Park, C.-S. Hwang, J. Jang and J. K. Jeong, *Appl. Phys. Lett.*, 2011, **99**, 102103.
3 B. S. Yang, S. Park, S. Oh, Y. J. Kim, J. K. Jeong, C. S. Hwang and H. J. Kim, *J. Mater. Chem.*, 2012, **22**, 10994.
4 Y. H. Hwang, H.-G. Im, H. Park, Y.-Y. Nam and B.-S. Bae, *ECS J. Solid State Sci. Technol.*, 2013, **2**, Q200.
5 K. K. Banger, R. L. Peterson, K. Mori, Y. Yamashita, T. Leedham and H. Sirringhaus, *Chem. Mater.*, 2014, **26**, 1195.
6 J.-S. Seo, J.-H. Jeon, Y. H. Hwang, H. Park, M. Ryu, S.-H. K. Park and B.-S. Bae, *Sci. Rep.*, 2013, **3**, 2085.
7 N. Itagaki, T. Iwasai, H. Kumomi, T. Den, K. Nomura, T. Kamiya and H. Hosono, *Phys. Status Solidi*, 2008, **205**, 1915.
8 A. Suresh and J. F. Muth, *Appl. Phys. Lett.*, 2008, **92**, 033502.
9 Y. H. Hwang, J.-S. Seo, J. M. Yun, H. Park, S. C. Yang, S.-H. K. Park and B.-S. Bae, *NPG Asia Mater.*, 2013, **5**, e4.
10 C. J. Brinker and G. W. Scherer, *Sol–Gel Science: The Physics and Chemistry of Sol–gel Processing*, Academic Press, 1990, ch. 2.
11 J. Livage, M. Henry and C. Sanchez, *Prog. Solid State Chem.*, 1988, **18**, 259.
12 W. W. Rudolph, D. Fischer, M. R. Tomney and C. C. Pye, *Phys. Chem. Chem. Phys.*, 2004, **6**, 5145.
13 W. W. Rudolph and C. C. Pye, *J. Solution Chem.*, 1999, **28**, 1045.
14 D. R. Lide, CRC Handbook of Chemistry and Physics, CRC Press, Inc., 1994, pp. 9–51.
15 B. Naik, K. M. Parida and C. S. Gopinath, *J. Phys. Chem. C*, 2010, **114**, 19473.
16 L. Szatmáry, S. Bakardjieva, J. Šubrt, P. Bezdičkaa, J. Jirkovskýb, Z. Bastlb, V. Brezovác and M. Korenkod, *Catal. Today*, 2011, **161**, 23.
17 E. C. Onyiriuka, *J. Non-Cryst. Solids*, 1993, **163**, 268.
18 M. M. Ennaceur and B. Terreault, *J. Nucl. Mater.*, 2000, **280**, 33.
19 J. F. Moulder, W. F. Stickle, P. E. Sobol and K. D. Bomben, *Handbook of X-ray Photoelectron Spectroscopy*, Perkin-Elmer Corporation, 1992, vol. 45.
20 T. T. John, C. S. Kartha, K. P. Vijayakumar, T. Abe and Y. Kashiwaba, *Appl. Surf. Sci.*, 2005, **252**, 1360.
21 C. Vionery, Y. Chevolot, D. Léonard, B.-O. Aronsson, P. Péchy, H. J. Mathieu, P. Descouts and M. Gräzel, *Langmuir*, 2002, **18**, 2582.
22 R. K. Brow, *J. Non-Cryst. Solids*, 1996, **194**, 267.
23 T. Kamiya, K. Nomura and H. Hosono, *Sci. Technol. Adv. Mater.*, 2010, **11**, 044305.
24 R. B. M. Cross and M. M. D. Souza, *IEEE Trans. Device Mater. Reliab.*, 2008, **8**, 277.
25 J. K. Jeong, *Semicond. Sci. Technol.*, 2011, **26**, 034008.
26 T.-C. Chen, T.-C. Chang, C.-T. Tsai, T.-Y. Hsieh, S.-C. Chen, C.-S. Lin, M.-C. Hung, C.-H. Tu, J.-J. Chang and P.-L. Chen, *Appl. Phys. Lett.*, 2010, **97**, 112104.
27 F. R. Libsch and J. Kanicki, *Appl. Phys. Lett.*, 1993, **62**, 1286.
28 T. Jun, K. Song, Y. Jung, S. Jeong and J. Moon, *J. Mater. Chem.*, 2011, **21**, 13524.
29 K. Ghaffarzadeh, A. Nathan, J. Robertson, S. Kim, S. Jeon, C. Kim, U.-I. Chung and J.-H. Lee, *Appl. Phys. Lett.*, 2010, **97**, 113504.
30 J. K. Jeong, *J. Mater. Res.*, 2013, **28**, 2071.
31 R. Asokamani and R. Manjula, *Phys. Rev. B: Condens. Matter Mater. Phys.*, 1989, **39**, 4217.

